Grain Growth and Coarsening Dynamics in a Compositionally Asymmetric Block Copolymer Revealed by X-ray Photon Correlation Spectroscopy

Ronald M. Lewis III,[1] Grayson L. Jackson,[2] Michael J. Maher,[1] Kyungtae Kim,[1] Suresh Narayanan,[3] Timothy P. Lodge,[1,4] Mahesh K. Mahanthappa,[1,] and Frank S. Bates[1,*]*

[1]Department of Chemical Engineering and Materials Science, University of Minnesota, Minneapolis, MN 55455, USA
[2]Department of Chemistry, University of Wisconsin–Madison, Madison, WI 53706, USA
[3]Advanced Photon Source, Argonne National Laboratory, Argonne, IL 60349, USA
[4]Department of Chemistry, University of Minnesota, Minneapolis, MN 5 5455, USA

**To whom correspondence should be addressed:* bates001@umn.edu; maheshkm@umn.edu

TOC Graphic

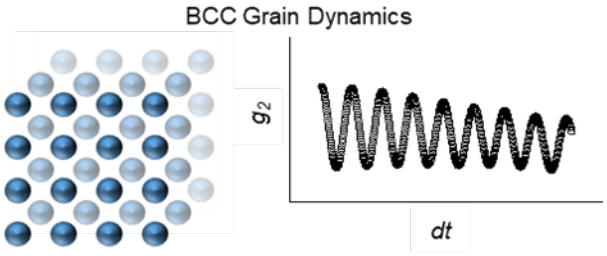

ABSTRACT

The dynamics of nanostructured soft materials crucially impact their associated macroscopic material properties, yet they are often difficult to measure due to spatiotemporal limitations of conventional instrumentation. Herein, we use X-ray photon correlation spectroscopy (XPCS) to directly observe particle-scale dynamics during grain growth and coarsening in a BCC-forming diblock polymer melt, with specific attention to the distribution of structural relaxation times associated with the interplanar (110) distance. Following sample quenching from the disordered state, these dynamical phenomena surprisingly exhibit little dependence on time and thermal quench depth. We posit that these relaxations stem from collective particle motions during grain rotation. We also observe unusual internally-referenced heterodyne correlations, which enable measurements of speed distributions within the sample. These speeds are significantly slower and appear at much longer annealing times than those previously reported during grain nucleation and growth in microphase separated block polymer melts. Drawing on analogies between polycrystalline hard and soft materials, we ascribe these speed distributions to misorientation-dependent grain boundary migration during ordered domain coarsening and anomalously fast, cooperative string-like particle motion along the grain boundaries. Thus, these coherent X-ray measurements provide new opportunities to interrogate grain boundary structure and dynamics in polycrystalline soft materials.

INTRODUCTION

The macroscopic properties of all polycrystalline materials depend sensitively on the spatially periodic arrangements of their constituents as well as the associated grain boundary (GB) structures and dynamics. As a result of techniques such as electron microscopy,[1–3] which enable direct visualization of atoms and GBs, GB engineering has long been a focal point of hard condensed matter. At much larger length scales, recent studies have employed light microscopy to investigate analogous GB behavior in crystals formed by immutable, micron-scale hard sphere colloids.[4,5]

Fewer techniques are available to study GB behavior in nanostructured soft materials. For self-assembled block polymers, analytical methods such as dynamic mechanical spectroscopy[6,7] and various forms of polarized light[8,9] or X-ray scattering[10–12] enable investigations of grain nucleation and growth from initially disordered polymer melts and solutions. However, these methods struggle to characterize processes associated with grain coalescence and refinement. While Bockstaller and coworkers recently used electron microscopy to characterize local grain coarsening in lamellar block polymers,[13,14] significant needs remain in the development of complementary scattering techniques to study the bulk dynamics of ordered mesoscopic grain coarsening in microphase separated block polymers.

X-ray photon correlation spectroscopy (XPCS) is a non-invasive technique that probes dynamic phenomena at nanometer length scales in disordered and ordered soft materials,[15–17] and is thus well-suited for studies of GBs. In block polymers, XPCS has been used to probe dynamics in the fluctuating disordered melt state,[15,18,19] with more recent work extending to ordered, microphase separated structures.[16,20,21] Patel *et al*. used XPCS to probe the effect of ordering on

'micelle relaxation times' during thermal quenches of a compositionally asymmetric diblock polymer into a hexagonally-packed cylinders (HEX) phase.[20] Sanz *et al*. observed a diffusive relaxation mode for ordered lamellar diblocks that they attributed to interfacial chain diffusion.[21] These results differ from recent reports by Hallinan and coworkers, who reported a hyperdiffusive relaxation mode in strongly segregated lithium salt-doped lamellar diblocks, which they ascribed to grain rotation.[16] However, no studies have yet used XPCS to investigate the dynamics associated with micellar sphere-packings such as the canonical body-centered cubic (BCC) morphology.

Herein we utilize XPCS to investigate the dynamics of a compositionally asymmetric diblock copolymer melt that forms BCC domains below the order-disorder transition temperature (T_{ODT}). Our previous report examined the early time behavior and relatively fast relaxations associated with the fluctuating disordered state of the same sample.[18] Here we focus on much longer-time relaxation processes and dynamics associated with the ordered BCC domains. Upon quenching the disordered sample to $T < T_{ODT}$, we obtain small-angle X-ray scattering (SAXS) patterns indicative of polycrystalline BCC order. Following our recently reported analytical framework for XPCS data obtained from such polycrystalline materials,[22] we extract a plethora of dynamic information as functions of thermal quench depth and annealing time. Long after initial phase nucleation and growth, we observe a distribution of structural relaxation times associated with the (110) interplanar distance that we ascribe to grain rotation. We also observe unique internally-referenced heterodyne correlations that enable extraction of speed distributions, with pronounced modes at u = 0.01 Å/s and 0.1 Å/s. This heterodyne scattering apparently stems from mixing of Bragg diffraction (internal reference speckle) with a fluctuating particle speckle pattern. Based on considerations of potential physical mechanisms, we hypothesize that these speed distributions arise from intensity fluctuations associated with misorientation-dependent GB

migration. An anomalously fast mode at u = 15 Å/s is also observed, which we speculate stems from cooperative, string-like motion of particles along high-angle GBs. The rich and complex GB dynamics uncovered in this study highlights XPCS as a powerful method for investigating mesoscale grain coarsening phenomena in polycrystalline soft materials.

Experimental

Polymer Synthesis. The diblock polymer sample under investigation was synthesized by anionic polymerization and characterized as described elsewhere.[23] Briefly, anhydrous and anaerobic styrene and butadiene monomers were sequentially polymerized in dry cyclohexane at 40 °C using a *sec*-butyl lithium initiator under air-free conditions to generate a low dispersity poly(styrene-*block*-1,4-butadiene) (PS-PB) diblock polymer with M_n = 28.6 kg/mol, $Đ = M_w/M_n$ = 1.03, and poly(butadiene) volume fraction f_{PB} = 0.20.[18]

SAXS Characterization. Samples were hermetically sealed in aluminum pans under inert atmosphere. SAXS measurements performed at Sector 5-ID-D of the Advanced Photon Source of Argonne National Laboratory revealed a microphase-separated body-centered cubic (BCC) structure at $T < T_{ODT}$ = 153 ± 1 °C, with a temperature invariant lattice constant a = 26 nm (additional sample characterization information is given in Ref. 18).

XPCS Data Collection and Analysis. Figure 1 illustrates the XPCS measurement protocol used in this report at the 8-ID-E beamline of the Advanced Photon Source at Argonne National Laboratory. The sample was first loaded into a 3 mm diameter, 3 mm thick stainless steel fluid cell with Kapton® windows and heated to 170 °C for 2 min. At this temperature, the system exists in a disordered state with composition fluctuations attributed to freely flowing, discrete particles

(micelles) that are unconstrained by any lattice symmetry.[18,24] This disordered sample was then transferred to the sample stage, which had been pre-equilibrated at a target quench temperature $T < T_{ODT}$. The temperature was maintained to within ± 1 °C by resistive heating and Peltier cooling elements. XPCS data acquisition with a frame rate of 1 Hz commenced on the sample immediately following the quench (t = 0 s) at a random position in the sample over intervals of 1000 s. As depicted in Figure 1, each subsequent measurement was performed at a different location in the sample to mitigate degradation induced by X-ray exposure (the beam impinges on a 20 μm x 20 μm square area).

XPCS data from the polycrystalline sample were processed using the previously reported analytical framework (see Ref. 22 and Supporting Information). The region on the area detector in the vicinity of the (110) reflection of the polydomain sample at $q^* = 0.0334 \pm 0.0005$ Å^{-1} was split into 750 azimuthal bins of approximately 100 detector pixels each, and the intensity in each bin was linearly correlated through time to generate the intensity-intensity autocorrelation function $g_2(t)$. These autocorrelation functions took multiple forms, the most common of which was a conventional single relaxation that was modeled using a Kohlrausch-Williams-Watts (KWW) form, $g_2(t) = b + c \cdot \exp(-(t/\tau)^{\beta})$. Other autocorrelation function types included a variety of heterodyne correlations, which were identified according to the procedures and definitions outlined in Ref. 22 and in the Supporting Information. Finally, we also observed some correlations that were too noisy to fit, which were labeled 'weak intensity grains.'

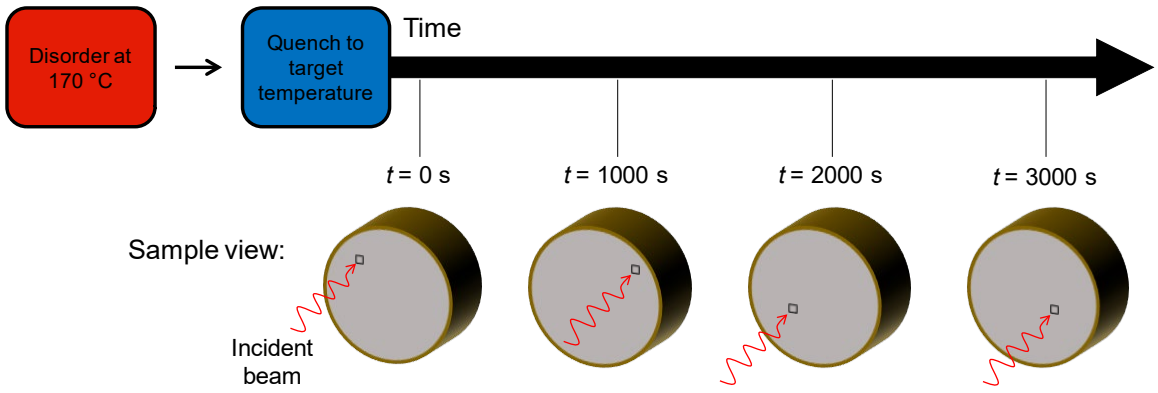

Figure 1. Schematic of XPCS experiments following the dynamic evolution of a BCC-forming block polymer. After rapidly quenching the disordered sample to a target temperature $T < T_{ODT}$, XPCS measurements were performed over 1000 s intervals to probe ordering and grain coarsening in the resulting BCC polycrystal. The cartoon sample views are not to scale.

RESULTS AND ANALYSIS

XPCS was used to study the temporal evolution of micelle scale dynamics of the BCC-forming PS-PB diblock polymer melt upon quenching from the disordered state. As functions of time and quench depth, we recorded several types of autocorrelation functions associated with the (110) primary scattering peak position $q^* = 0.0334 \pm 0.0005$ Å^{-1}. Using our previously developed analytical framework,[22] these correlations were classified as 'weak intensity grain,' 'complex heterodyne,' 'clean heterodyne,' 'low frequency heterodyne,' 'single relaxation,' and 'both low and single.' The time and temperature evolutions of these classifications at various temperatures below T_{ODT} are provided in Figure 2 (Figure S1 furnishes higher resolution charts at each temperature).

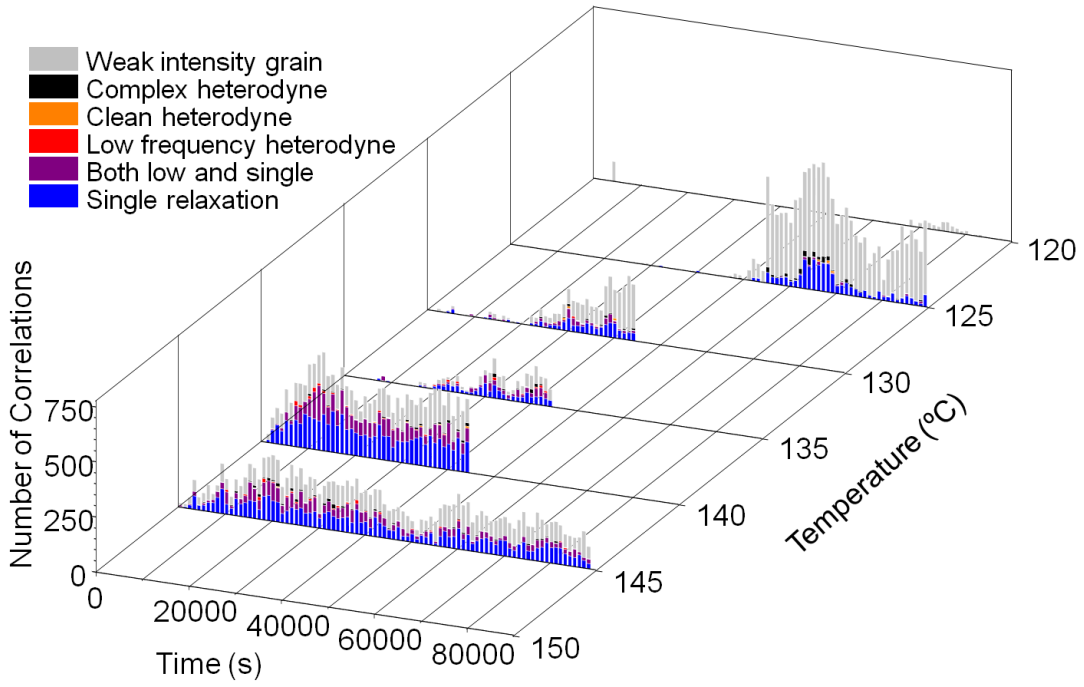

Figure 2. Temperature-dependent XPCS measurements of the BCC-forming diblock (T_{ODT} = 153 ºC) obtained as a function of time at the (110) reflection $q^* = 0.0334 \pm 0.0005$ Å^{-1}, following thermal quenches from 170 ºC. The times at which grains begin to form at each temperature qualitatively agree with previous dynamic studies regarding nucleation and growth of order in this sample.[18] At 120 ºC, the sample apparently becomes non-ergodic and no large-domain BCC growth is observed during the XPCS measurement. The ordering kinetics for this diblock polymer suggested that a measurement duration of 45,000 s was sufficient to capture nucleation and growth at 130 ºC, 135 ºC, and 140 ºC, whereas data was acquired at 125 ºC and 145 ºC over 90,000 s.

We attribute all of the correlations shown in Figure 2 to dynamic processes of particles ordered in BCC grains (*i.e.* 'on grain'), based on several pieces of evidence. First, the times required for these 'on grain' correlations to appear at each temperature concur with rapid increases in the dynamic elastic modulus (G') recorded by dynamic mechanical spectroscopy (DMS) measurements on this sample (see Figure S2 and Ref. 18), which are associated with particle ordering. Second, there exist no 'on grain' correlation functions at T = 120 °C. This observation is consistent with the uniform azimuthal intensity at q^* at T = 120 °C (Figure 3A) after ~25 h of

isothermal annealing, which indicates that grains present in this non-ergodic regime are much smaller in size than the incident X-ray beam. Figure S3 shows that the azimuthally-averaged SAXS intensity exhibits a relatively broad principal peak at q^* and a very weak, second order (200) reflection indicative of marginal translational order. The nearly isotropic scattering ring at q^* obtained at $T < 125$ °C, which evidences a strong fixed correlation length between particles, markedly contrasts the 'spotty' SAXS diffraction patterns observed at $T = 130–145$ °C, where we expect conventional nucleation and grain growth to predominate (Figure 3B). In addition to the 2D X-ray patterns in Figure 3, Figure S3 furnishes additional evidence of the time-dependent variations in azimuthal intensity with quench temperature. We also note that lower intensities and 'spotty' reflections prevented similar analysis of higher order reflections due to statistical limitations.

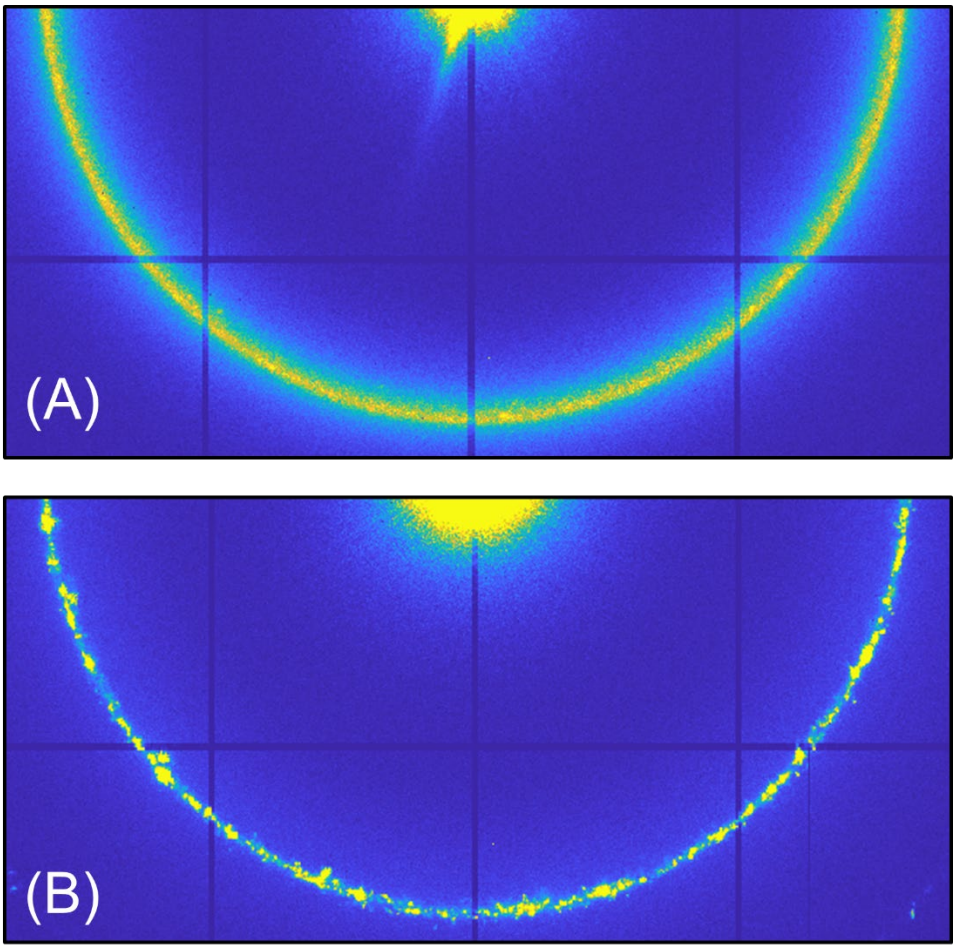

Figure 3. 2D-SAXS patterns acquired at (A) 120 °C and (B) 145 °C after annealing at each temperature for approximately 25 h plotted on identical logarithmic color scales. A dearth of long-range order at low temperature in (A) produces almost no variation in intensity, whereas the presence of many sizable BCC grains at higher temperature in (B) led to a 'spotty' intensity at q^*. Figure S3 provides the time evolution of the azimuthally-averaged intensity along with 1D integrated patterns corresponding to these images.

We first focus on the XPCS data for single, KWW-type exponential relaxations. Following quenches to various $T < T_{ODT}$ that are associated with different nucleation and growth regimes for this PS-PB diblock (Figure S2), KWW fits reveal a distribution of relaxation times at each temperature as shown in Figure 4. In > 99 % of the cases, compressed exponentials with $\beta > 1$ adequately fit the correlations (Figure 5), in agreement with prior reports of confined or non-Brownian particle motion in other soft materials,[25,26] and specifically lamellar block polymers.[16]

Note that this sample exhibits very weak scattering intensity for $q \neq q^*$ (see Figure S3), thus we are unable to probe the q-dependence of the structural relaxation times. The relaxation time distributions were assumed to be Gaussian and fits to the distributions through time yielded mean relaxation times $\bar{\tau}$ and standard deviations (Figure S4). The final average relaxation times are shown in the bottom right panel of Figure 4 as a function of quench temperature.

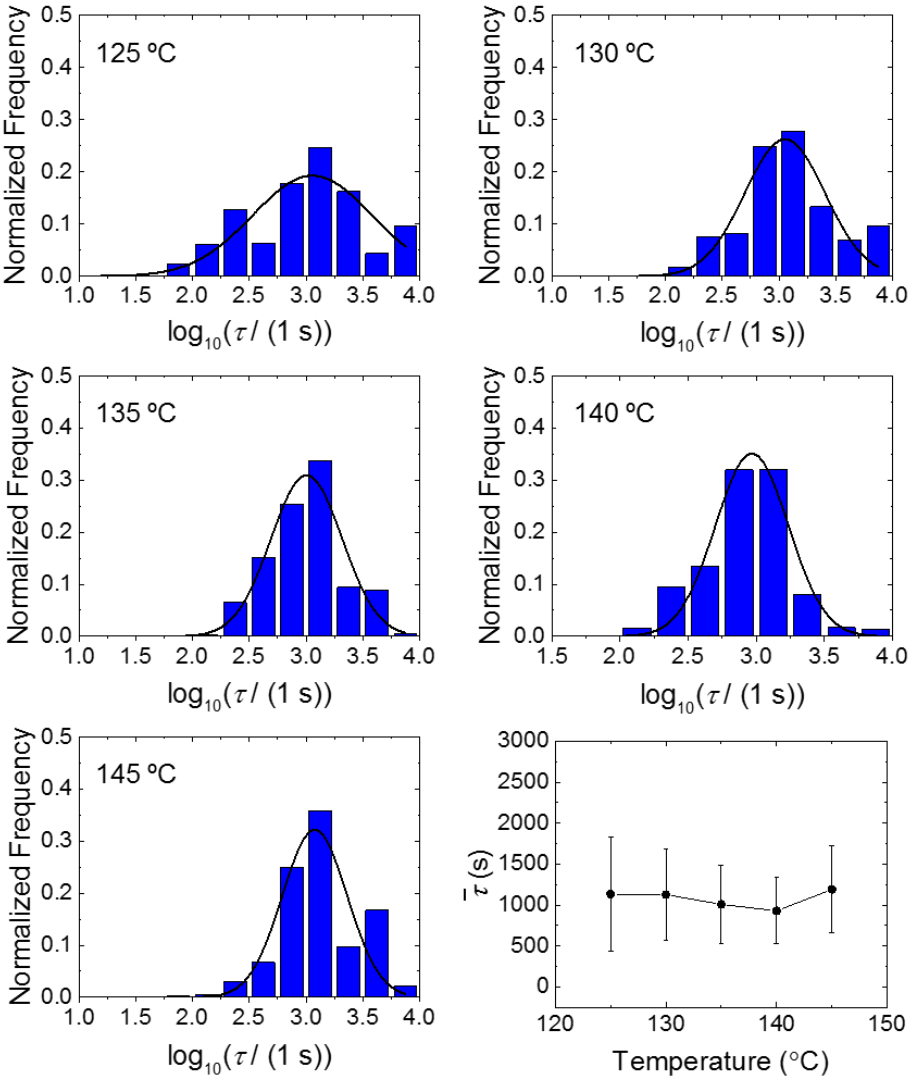

Figure 4. Final cumulative particle relaxation time distributions as a function of quench temperature ($N > 700$ correlations, the sum of all blue data in Figure 2). The right-most bin at $\log_{10}(\tau/(1\text{ s})) = 3.75$ contains all instances of $\tau \geq 10^4$ s. The solid lines are Gaussian fits to the

distributions. The mean relaxation time from these fits is plotted versus quench temperature in the bottom-right panel.

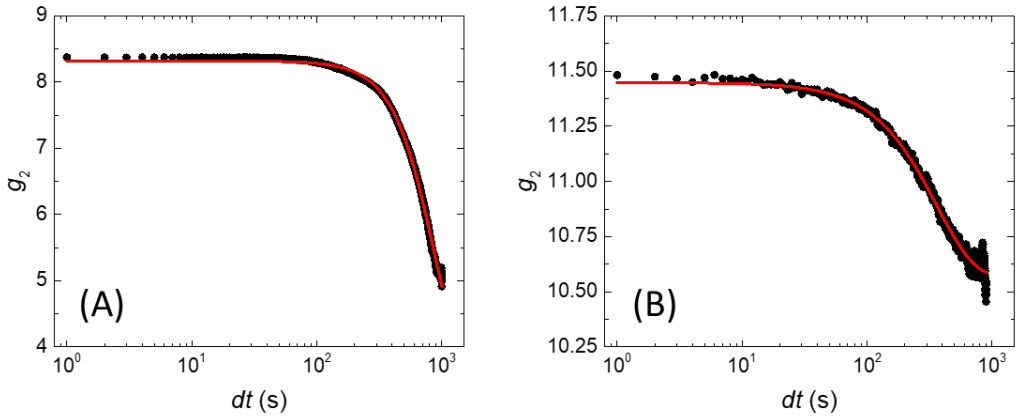

Figure 5: Data (*black circles*) and fits (*red lines*) of conventional correlation functions obtained after annealing for approximately 24 hours following quenches from disorder. For the correlation function at 125 °C (A), $\tau = 1150 \pm 20$ s and $\beta = 2.27 \pm 0.03$. At 145 °C (B), $\tau = 580 \pm 10$ s and $\beta = 1.43 \pm 0.04$.

The average relaxation times remain nearly constant at approximately $\bar{\tau} \approx 1000$ s for all quench temperatures, suggesting that the dominant relaxation mode measured by XPCS is independent of temperature. Consistent with prior XPCS studies of ordering in block polymers,[20,21] the 'on grain' structural relaxations are much longer than those that we previously reported for the supercooled fluctuating disordered state of this system.[18] The order of magnitude increase in the structural relaxation times upon ordering implies a change in mechanism from one dominated by diblock polymer chain exchange between micelles in the disordered state (prior to ordering after supercooling from 170 °C to $130 < T < 153$ °C) to another mode of relaxation likely tied to the ordered domain dynamics. Our results are also comparable to structural relaxations measured by XPCS for strongly segregated lamellar poly(styrene-*block*-ethylene oxide) block polymers.[16]

However, the relaxation time measured by Oparaji *et al.*[15] showed an Arrhenius temperature dependence, whereas those in this study exhibit very weak temperature dependences. We return to this point below.

In addition to conventional relaxation times obtained from KWW fitting, we also observed unique heterodyne correlations at T = 125–145 °C. While most systems require a stationary external reference to generate heterodyne scattering,[27] the heterodyne correlations displayed by the BCC ordered PS-PB material are internally referenced, indicative of two sources of scattering of comparable scattering intensity that are moving relative to each other.[22,28–30] The framework used to identify, classify, and fit XPCS heterodyne correlations for this polycrystalline sample was developed previously[22] and is outlined in the Supporting Information. A characteristic frequency ω associated with each internal particle speed $u = \omega/q^*$ was extracted by combinations of fast Fourier transform analysis and fitting to mathematical models of heterodynes.[29] Figure 6 depicts representative examples of slow (0.020 Å/s), intermediate (0.31 Å/s), and fast (≥ 15 Å/s) heterodyne correlation functions (see Figure S5 for additional examples).

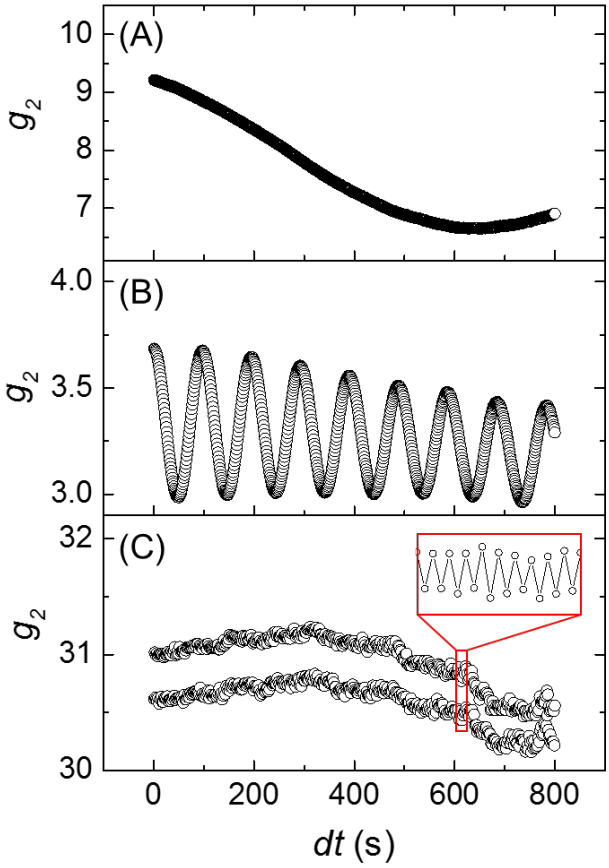

Figure 6. Representative heterodyne correlation functions: (A) a low frequency heterodyne with $\omega = 0.00065$ s^{-1} ($u = 0.020$ Å/s) after annealing the sample at 130 ºC for ~ 9 h, (B) a heterodyne with $\omega = 0.010$ s^{-1} ($u = 0.31$ Å/s) after annealing the sample at 130 ºC for ~ 8.3 h, and (C) an instrument resolution-limited heterodyne with $\omega \geq 0.5$ s^{-1} ($u \geq 15$ Å/s) obtained after annealing the sample at 145 °C for ~ 8 h.

Beyond other established metrics of sample stability,[18] the constant speeds observed over the 1000 s experiment indicate that these heterodyne correlations are not measurement artifacts. Additionally, two-time correlation analysis suggests that the dynamics are relatively constant over the course of the entire measurement (see Figure S6). For clarity, we first discuss the cumulative speed distributions before considering their physical origins. Importantly, the vast majority of heterodyne correlations do not appear until long after nucleation and growth has occurred on the basis of DMS measurements (Figure S2), suggesting these speeds only manifest after the sample

has developed a polycrystalline grain texture. This is evidenced by Figure 7, which shows the total number of speeds measured as a function of the percentage of mesoscopic crystalline order in the sample measured by DMS.

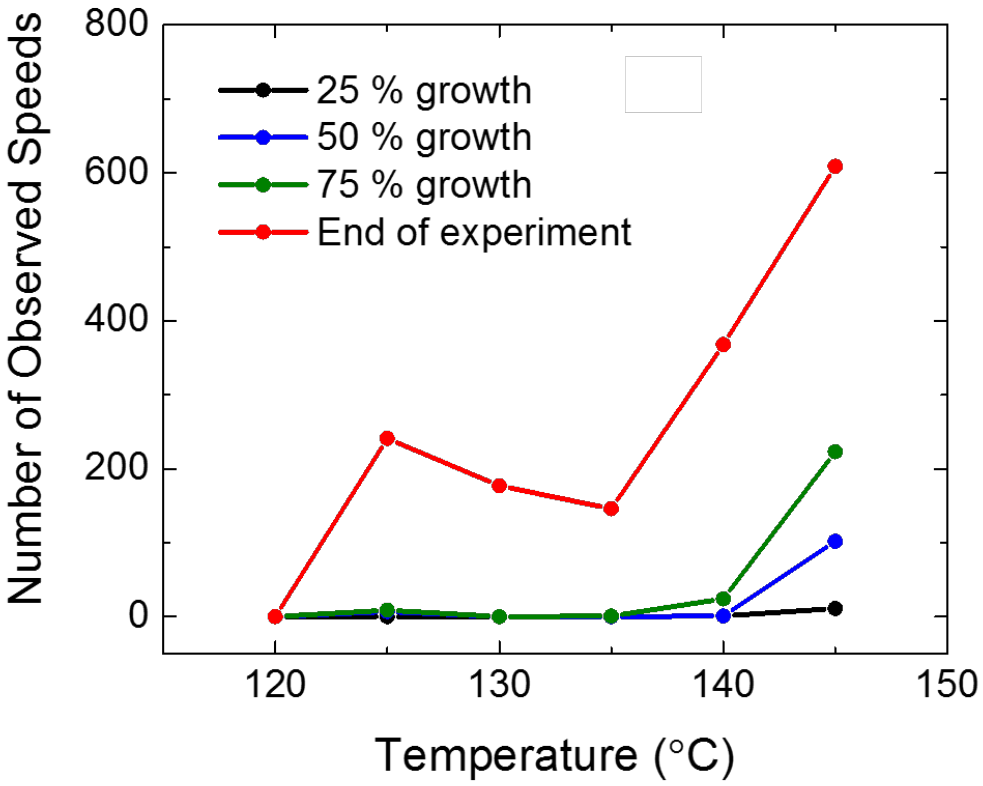

Figure 7: The total number of observed internally referenced speeds at different growth times as a function of temperature. At 120 °C, no heterodyne signals were observed. The percentage of grain growth is taken as the point at which the elastic modulus reached 25 %, 50 %, and 75 % of its maximum value following quenches from disorder (see Figure S2). The number of speeds increases dramatically between 75 % growth and the end of the experiment at all temperatures, suggesting this phenomenon relates to inter-grain interactions.

In Figure 8 we plot the cumulative speed distributions from heterodyne scattering as a function of quench temperature. These distributions are representative of the entire sample, *i.e.* they are not limited by selective sampling, as each distribution comprises > 150 observed speeds

(Figure 7). Moreover, the number of histogram bins was chosen to uniformly represent the data at all temperatures based on the number of speeds present. By fitting a single Gaussian to the distribution at 125 °C, we observe a sharp unimodal peak with an average speed of ~ 0.1 Å/s. While higher quench temperatures led to narrower distributions of $\bar{\tau}$ (Figures 4 and S4), the cumulative speed distribution broadens at 130 °C and, above this temperature, splits into a multimodal distribution with a new 'slow' mode appearing at ~0.01 Å/s (green arrows in Figure 8). Limited degrees of freedom based on the number of bins used for the multimodal distributions prevented reliable use of multiple Gaussian fits. The cumulative speed distribution is essentially constant when $135 \leq T \leq 145$ °C. At the highest quench temperature, we observe several instances of a fast mode with speeds ≥15 Å/s (blue arrow in Figure 8), with the lower bound set by the instrument resolution (Figure 6C inset). While the observed speed distributions may be subject to error associated with Doppler phase shifting in the beam direction, these variations are $O(1)$ and cannot alone explain the apparent multimodal speed distributions that span multiple orders of magnitude.

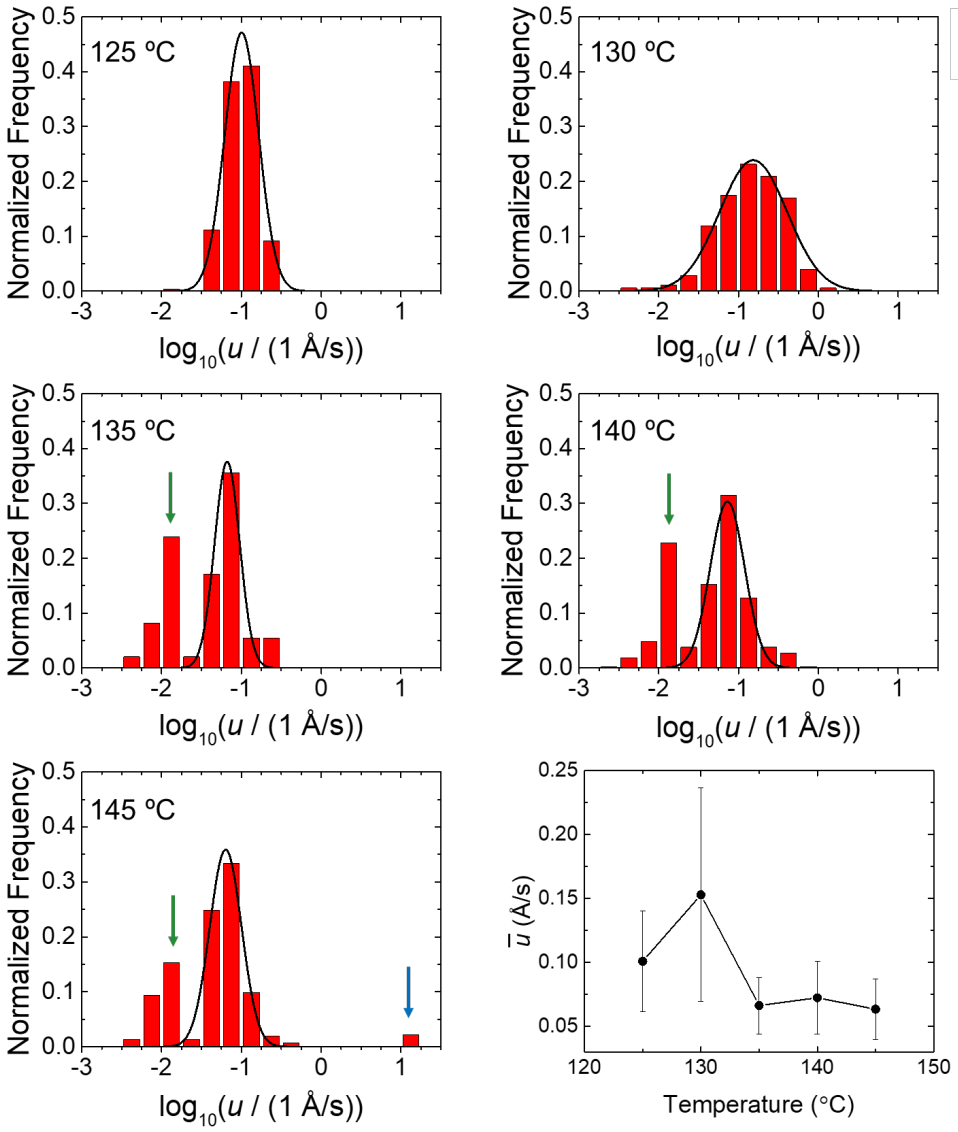

Figure 8. Final cumulative speed distributions derived from heterodyne scattering as a function of quench temperature, in which the solid lines are Gaussian fits to the distribution centered on the intermediate speed mode. Green arrows at 135 ºC, 140 ºC, and 145 ºC indicate the emergence of a slow speed mode, and the single blue arrow at 145 ºC points to the fastest speed mode. The bottom-right plot depicts the temperature-dependence of the average cumulative speeds.

DISCUSSION

XPCS reveals a rich dynamic portrait of the polycrystalline BCC diblock polymer material during grain nucleation, growth, and coarsening. We observe a distribution of structural relaxations that can be fit using the 'compressed' KWW function with $\beta > 1$. The average relaxation times $\bar{\tau}$ are approximately 1000 s and exhibit virtually no temperature dependence. We also observe internally-referenced heterodyne scattering that is constant over the course of the entire 1000 s measurement, as evidenced by the two-time correlations shown in Figure S6. From these heterodyne correlations, we extracted speed distributions within this sample. These dynamic processes are only observed long after initial nucleation and growth of BCC order (Figure 7). In other words, the sample has already developed a full polycrystalline texture by the time we observe 'on grain' structural relaxations and heterodyne correlations.

The structural relaxations measured by XPCS result from intensity fluctuations of the (110) Bragg peak and thus reflect physical processes that either: (1) cause fluctuations in the (110) interplanar distance, or (2) alter the orientation of {110} planes with respect to the beam by grain rotation. One potential mechanism consistent with the first process is relaxation of interstitial defects or vacancies generated during the initial quenching process. However, we anticipate that the concentration of such intrinsic defects is relatively low due to the constraint of filling space at constant density, and therefore this effect should not contribute significantly to the fluctuating scattered intensity. Substantial fluctuations in the (110) interplanar distance may also be caused by fluctuations in micelle size resulting from individual chain exchange events, by analogy to the lamellar diblock polymers studied by Sanz *et al*.[21] However, we previously measured considerably faster relaxation times in the fluctuating disordered state of this same system prior to BCC grain nucleation that are associated with block polymer chain exchange events.[18] The order of magnitude

longer relaxation times in the ordered state likely implies that the physical mechanism of structural relaxation is caused by longer-ranged, collective motion. We note that this collective motion may be mediated by chain exchange events in the ordered state, where the energetic penalty for particle volume perturbations is greater than in the disordered state, and therefore particle relaxation times may become longer. However, the observed temperature independence of the relaxation time distributions is not expected for chain exchange mediated relaxation, which we anticipate would reflect the segregation strength of the system,[31] thus ruling out this mechanism.

It is possible that the observed relaxations stem from lattice vibrations that propagate through the sample, which cause fluctuations in the (110) interplanar distance in a manner comparable to phonons in metals. A rudimentary 1D classical calculation can be performed to approximate the phonon relaxation time based on the elastic modulus (G') of the material, the density ρ, and a relevant length scale (a) according to $\tau^2 \propto \frac{\rho a^2}{G'}$.[32] With G' ~ O(10^4) Pa,[18] ρ ~ O(10^3) kg/m^3, and the lattice parameter a ~ O(10^{-8}) m, this relationship yields a relaxation time of order 10^{-9} s. This result qualitatively agrees with several reports that establish phonon dynamics in a variety of comparable soft materials,[33–36] and thus we surmise that phonon modes are not a likely cause of the relaxation times recorded in this report.

We consequently speculate that the most likely source of structural relaxation in our system is grain rotation. Grain rotation physically results from a net torque on a grain due to the misorientation-dependent energy of its surrounding GBs. As pointed out by Hallinan and coworkers, this long-range cooperative motion would account for the large intensity fluctuations measured by XPCS.[16] The orientation of the {110} layers with respect to the incident X-ray beam determines the scattering cross-section, and the scattered intensity oscillates between conditions

of maximal and minimal scattering extremes as the grain rotates. Based on this phenomenon, scattering intensity fluctuations have been used to directly measure the rotation rates of nanoparticles during *in situ* TEM experiments.[37] Beyond providing the requisite intensity fluctuations, grain rotation is known to occur during thermal annealing and has been observed by TEM for polycrystalline metallic films[38,39] and in lamellar block polymers.[14]

The structural relaxation time distributions offer physical insights into the polycrystalline structure of the BCC sample. Theoretical descriptions of grain rotation indicate that the rotation rate scales as d^{-4} where d is the grain diameter, when grain rotation is primarily accommodated by particle diffusion along GBs.[40] While one would intuitively expect grain rotation rates to increase with temperature, as noted by Hallinan and coworkers,[16] the average relaxation time in our system exhibits no temperature dependence. Scherrer analysis and Figure 3 (see Table S2) demonstrate that the grain size is generally smaller at lower temperatures, which should lead to faster rotation rates. However, this effect could be partially counterbalanced by the increased relaxation time of the particle corona blocks and/or the formation of a larger population of more irregularly shaped grains at the reduced temperatures. A strong sensitivity to grain size suggests that the broader structural relaxation distribution (*e.g.*, rotation rates) at T = 125 °C (Figures 4 and S4) directly reflects a broader grain size distribution in this non-ergodic regime. By this same reasoning, the narrower relaxation time distributions at higher temperatures may reflect a more uniform grain size distribution.

We now consider potential physical phenomena that may give rise to heterodyne correlations in our system. Gabriel *et al*. recently demonstrated how temperature gradients affect correlation experiments, wherein compressed exponential relaxations could be accounted for by assuming a constant velocity convective flow.[41] In the present system, one could imagine that a

constant flow velocity due to *convective* heat transfer could cause entire grain motion and lead to the observed heterodyne correlations. However, a rudimentary calculation of the Rayleigh number suggests that thermal equilibration in our sample is instead dominated by *thermal conduction* (see Supporting Information for calculations). Conductive heat transfer is also consistent with the physical, non-flowing state of the structured solid sample below the ODT, for which we observe higher elastic contributions to the modulus at all temperatures.[18] Therefore, we rule out the notion of convective grain movement as the source of heterodyne speeds in our experiments.

Prior reports of block polymer grain growth rates following quenches from disorder to $T < T_{ODT}$ have noted comparable velocities to those in the current system.[8,13,42–44] On the basis of work by Liebig and Fredrickson, Balsara and coworkers developed an expression for the grain growth front velocity, $v = (R/\alpha)[\chi N - (\chi N)_{ODT}]g(f)$, where R is the root mean-square end-to-end length of the diblock polymer, α is the longest relaxation time of the chains, χN is the temperature dependent segregation strength ($\chi \sim T^{-1}$), and $g(f)$ is an $O(1)$ shape factor.[42,45,46] These parameters were determined previously for this system,[18,23] enabling calculation of grain growth front velocities ranging from 4 – 60 Å/s for different quench depths (see Supporting Information for details). Our estimates also concur with simulations by Spencer *et al*. for BCC-forming block polymers quenched from the disordered state ($v \approx 60R_g/\tau \gtrsim 10$ Å/s).[44] However, both the order of magnitude and temperature independence of our observed speed distributions conflict with the grain growth rates estimated using both established methods (Figure 9). Consistent with this notion, heterodyne correlations appear much later than the initial grain nucleation and growth processes established by DMS (Figure S2). In other words, the vast majority of initially disordered particles have been incorporated into the polycrystalline texture before we observe heterodyne scattering. This inference distinguishes the current work from that of Headrick and coworkers,[30,47]

where surface propagation relative to stationary bulk defects gave rise to XPCS heterodyne scattering; this mechanism is excluded here.

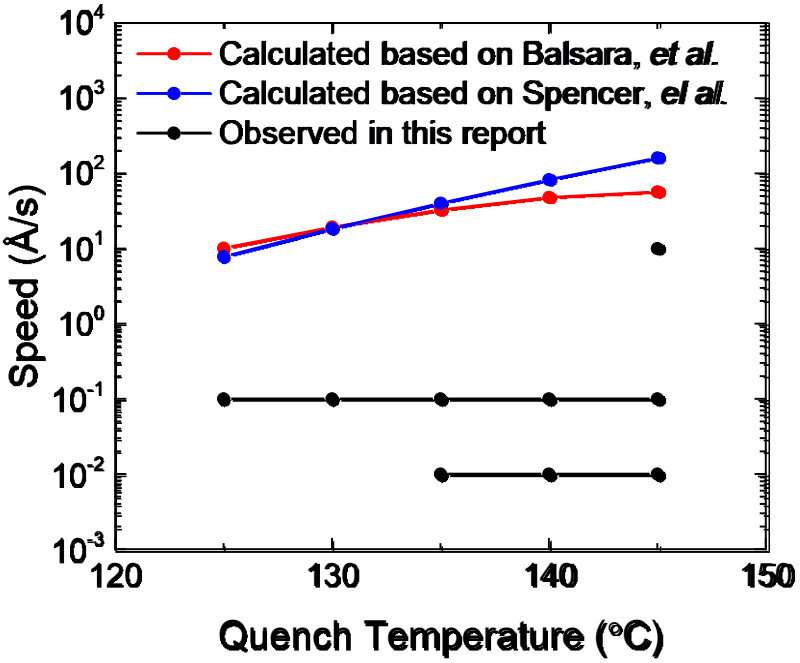

Figure 9. Comparison of observed speeds documented in this report and the calculated grain growth front velocities (red and blue curves), details of which are furnished in the Supporting Information. The disparity between the observed and calculated speeds suggests that grain growth is not the mechanism responsible for the heterodyne signals observed here.

In lieu of nucleation and growth mechanisms, we speculate that the dominant velocities in the polycrystalline sample are due to defect migration throughout the bulk of the grains or GB migration. The internal referencing of heterodyne correlations at q^* strongly suggests that the well-defined (110) interplanar distance within BCC grains serves as the 'stationary' internal reference required for the observation of heterodyne scattering. Internally-referenced heterodyne scattering in XPCS experiments also requires the scattering intensity of the moving object to be comparable to that of the stationary reference;[29] we do not anticipate the scattering associated with bulk defects

moving throughout our sample to be comparable to that associated with (110) diffraction. In contrast, the more correlated motion of micellar particles at GBs within our polycrystalline sample is a more likely candidate for the observed speeds. Furthermore, our measured GB migration rates compare favorably with results from Lodge and coworkers, who reported an average grain growth rate of 4 Å/s for the BCC → FCC transition in block polymer lyotropic liquid crystals.[48] We expect GB mobilities in the latter case to be generally faster than in the melt, consistent with the notion that our measured speeds are due to GB migration during coarsening.

We posit that the speeds in our measurement may stem from two distinct yet related coarsening phenomena: (i) grain boundary migration between misoriented grains in the polycrystal, which give rise to the main distribution of speeds, and (ii) cooperative particle motion along the grain boundary associated with the highest velocity mode of ~10 Å/s. Schematics for these potential modes are displayed in Figure 10. A number of studies have demonstrated that grain boundary mobility depends sensitively on the relative misorientation between adjacent grains, with low-angle grain boundaries (LAGBs) generally moving more slowly, and high-angle grain boundaries (HAGBs) migrating quickly due to their higher interfacial energies[13,49–51]. Accordingly, we assign the slow velocity mode $u_{LAGB} \approx 0.01$ Å/s to the LAGBs and the intermediate speed mode at $u_{HAGB} \approx 0.1$ Å/s to HAGB migration. In this light, the heterodyne frequency distributions in our XPCS measurement not only provide valuable information about GB dynamics but may also reflect the underlying distribution of GB misorientation angles within the coarsening polycrystal. It is tempting to interpret the bimodal GB speed (and misorientation) distributions in our system for $135 \leq T \leq 145$ °C as evidence for preferential GB migration along special {110} misorientation pairs, as the choice of a {110} rotation axis can transform a random distribution of GB misorientations into a similar bimodal distribution.[52] We therefore postulate

that for $135 \leq T \leq 145$ °C, our sample possesses a random distribution of GB misorientations. The bimodal heterodyne frequency disappears for $T \leq 130$ °C and the resulting unimodal speed distributions are centered at $u_{HAGB} \approx 0.1$ Å/s. We note that the transition from bimodal to unimodal speed distributions corresponds to a transition in the range of order from SAXS (Figure S3); hence the presence of LAGBs is tied to longer-range order. Extension of the GB dynamics argument presented here allows us to speculate that diffusion-limited growth in this non-ergodic low temperature regime leads to a larger population of HAGBs between BCC grains. We note that heterodyne correlations cease to appear as the quench temperature is decreased further to 120 °C. Presumably, this is a consequence of the complete lack of GBs due to suppression of microphase separated melt ordering below the ergodicity transition,[53] where liquid-like packing (LLP) dominates the morphology.

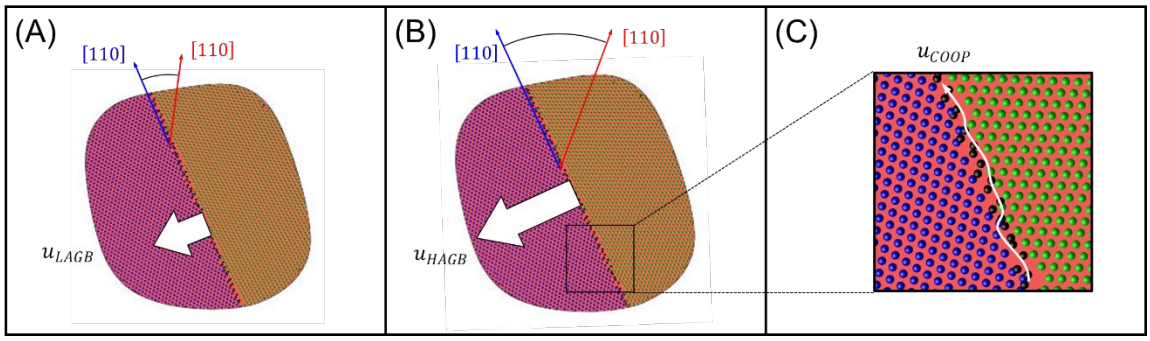

Figure 10. Schematic illustrations demonstrating the postulated origins of the three velocities (white arrows) that lead to heterodyne scattering signatures in the BCC-forming SB diblock polymer. Two BCC grains with low (A) and high (B) misorientation angles lead to distinct grain boundary speeds, u_{LAGB} and u_{HAGB}, associated with different grain boundary energies. In (C), the fastest speed mode corresponds to the cooperative, string-like motion of particles along the boundary.

While grain misorientation may account for the majority of the speed distribution, the highest velocity mode, only observed at 145 °C, is at least two orders of magnitude faster than the

intermediate mode and also much faster than the GB velocity of 4 Å/s measured by Lodge and coworkers in dilute polymer solutions.[48] In line with experimental and computational studies of other soft materials, we postulate that this mode corresponds to the cooperative, string-like movement of particles along HAGBs depicted schematically in Figure 10C, with characteristic speeds of $u_{COOP} \gtrsim 10$ Å/s.[5,54,55] Observation of this high frequency heterodyne correlation (velocity) over the entire 1000 s measurement implies particle movement of at least 1 μm, consistent with the average grain size arising from a simple Scherrer analysis of the data in Figure 3B (see Supporting Information). We note that the we cannot exclude other fast particle mechanisms for this apparent speed, such as distinct yet related 'crowdion' movements or dislocation 'avalanches.'[56–58]

CONCLUSIONS

In this report, XPCS measurements were conducted on a model BCC-forming diblock polymer at various quench temperatures below the T_{ODT}. We observed structural relaxations that we assign to grain rotation and used the width of the relaxation time distribution to infer a broader grain size distribution at lower temperatures. We also observed unique internally-referenced heterodyne correlations, from which we extracted velocity distributions within the sample. We postulate that these speeds reflect grain boundary (GB) misorientation in the polycrystalline material. In the nucleation-limited temperature regime ($135 \leq T \leq 145$ °C), larger average grain sizes lead to a random distribution of GB misorientations. Decreasing the quench temperature into the diffusion-limited regime ($T < 135$ °C) leads to smaller average grain sizes with a higher frequency of intermediate speeds, which we associate with HAGBs migration events. Finally, we

observe an anomalously fast, instrument resolution-limited mode that we postulate corresponds to rapid and cooperative particle displacement along the grain boundaries. The findings and analyses in this report highlight the power of XPCS in unveiling detailed dynamic and structural information in diblock copolymers with potential extensions to other soft and hard materials.

ASSOCIATED CONTENT

Supporting Information. Details and calculations of the XPCS analytical framework, two-time correlation functions, Rayleigh Number, grain growth velocity, and Scherrer analysis, and supporting Figures. This material is available free of charge *via* the Internet at http://pubs.acs.org.

AUTHOR INFORMATION

Corresponding Authors

*Email: bates001@umn.edu; maheshkm@umn.edu

Present Addresses

R.M.L.: 51 Glen Manor Lane, Glenmoore, PA, 19343

G.L.J.: James Franck Institute, University of Chicago, 929 E. 57th St., Chicago, IL 60637 USA

K.K.: Materials Physics and Applications Division, Center for Integrated Nanotechnologies, Los Alamos National Laboratory, Los Alamos, NM 87545

ORCID

Ronald M. Lewis III: 0000-0002-7388-4439

Grayson L. Jackson: 0000-0003-0663-3274

Michael J. Maher: 0000-0003-0577-3726

Kyungtae Kim: 0000-0002-3206-8494

Mahesh K. Mahanthappa: 0000-0002-9871-804X

Timothy P. Lodge: 0000-0001-5916-8834

Frank S. Bates: 0000-0003-3977-1278

Author Contributions

The manuscript was written through contributions of all authors. All authors have given approval to the final version of the manuscript.

Notes

The authors declare no competing financial interest.

Acknowledgment

Support for this work was provided by the National Science Foundation under Grants DMR-1801993 (R.M.L., M.J.M., K.K., and F.S.B.), CHE-1608115 and CHE-1807330 (G.L.J. and M.K.M.). SAXS experiments were conducted at the 8-ID-E and 5-ID-D Advanced Photon Source (APS). Use of the APS, an Office of Science User Facility operated for the U.S. Department of Energy (DOE) Office of Science by Argonne National Laboratory, was supported by the U.S. DOE under Contract No. DE-AC02-06CH11357.

REFERENCES

(1) Bowers, M. L.; Ophus, C.; Gautam, A.; Lançon, F.; Dahmen, U. Step Coalescence by Collective Motion at an Incommensurate Grain Boundary. *Phys. Rev. Lett.* **2016**, *116*, 1–5. https://doi.org/10.1103/PhysRevLett.116.106102.

(2) Huang, Y.; Humphreys, F. J. Measurements of Grain Boundary Mobility during Recrystallization of a Single-Phase Aluminium Alloy. *Acta Mater.* **1999**, *47*, 2259–2268. https://doi.org/10.1016/S1359-6454(99)00062-2.

(3) Huang, Y.; Humphreys, F. J. Subgrain Growth and Low Angle Boundary Mobility in Aluminum Crystals of Orientation {110}<001>. *Acta Mater.* **2000**, *48*, 2017–2030.

(4) Alsayed, A. M.; Islam, M. F.; Zhang, J.; Collings, P. J.; Yodh, A. G. Premelting at Defects Within Bulk Collodial Crystals. *Science.* **2005**, *309*, 1207–1210. https://doi.org/10.1126/science.1112399.

(5) Nagamanasa, K. H.; Gokhale, S.; Ganapathy, R.; Sood, A. K. Confined Glassy Dynamics at Grain Boundaries in Colloidal Crystals. *Proc. Natl. Acad. Sci.* **2011**, *108*, 11323–11326. https://doi.org/10.1073/pnas.1101858108.

(6) Adams, J. L.; Quiram, D. J.; Graessley, W. W.; Register, R. A.; Marchand, G. R. Ordering Dynamics of Compositionally Asymmetric Styrene-Isoprene Block Copolymers. *Macromolecules* **1996**, *29*, 2929–2938. https://doi.org/10.1021/ma951261+.

(7) Lee, S.; Leighton, C.; Bates, F. S. Sphericity and Symmetry Breaking in the Formation of Frank-Kasper Phases from One Component Materials. *Proc. Natl. Acad. Sci. U. S. A.* **2014**, *111*, 17723–17731. https://doi.org/10.1073/pnas.1408678111.

(8) Chastek, T. Q.; Lodge, T. P. Grain Shapes and Growth Kinetics of the Cylinder Phase in a Block Copolymer Solution. *Macromolecules* **2004**, *37*, 4891–4899. https://doi.org/10.1021/ma049502d.

(9) Newstein, M. C.; Garetz, B. A.; Balsara, N. P.; Chang, M. Y.; Dai, H. J. Growth of Grains and Correlated Grain Clusters in a Block Copolymer Melt. *Macromolecules* **1998**, *31*, 64–76. https://doi.org/10.1021/ma971086s.

(10) Harkless, C. R.; Singh, M. A.; Nagler, S. E.; Stephenson, G. B.; Jordan-Sweet, J. L. Small-Angle x-Ray-Scattering Study of Ordering Kinetics in a Block Copolymer. *Phys. Rev. Lett.* **1990**, *64*, 2285–2288. https://doi.org/10.1103/PhysRevLett.64.2285.

(11) Singh, M. A.; Harkless, C. R.; Nagler, S. E.; Shannon, R. F.; Ghosh, S. S. Time-Resolved Small-Angle x-Ray-Scattering Study of Ordering Kinetics in Diblock Styrene-Butadiene. *Phys. Rev. B* **1993**, *47*, 8425–8435. https://doi.org/10.1103/PhysRevB.47.8425.

(12) Nie, H.; Bansil, R.; Ludwig, K.; Steinhart, M.; Koňák, Č.; Bang, J. Time-Resolved Small-Angle X-Ray Scattering Study of the Kinetics of Disorder-Order Transition in a Triblock Copolymer in a Selective Solvent for the Middle Block. *Macromolecules* **2003**, *36*, 8097–8106. https://doi.org/10.1021/ma034357+.

(13) Ryu, H. J.; Fortner, D. B.; Rohrer, G. S.; Bockstaller, M. R. Measuring Relative Grain-Boundary Energies in Block-Copolymer Microstructures. *Phys. Rev. Lett.* **2012**, *108*, 1–5. https://doi.org/10.1103/PhysRevLett.108.107801.

(14) Ryu, H. J.; Fortner, D. B.; Lee, S.; Ferebee, R.; De Graef, M.; Misichronis, K.; Avgeropoulos, A.; Bockstaller, M. R. Role of Grain Boundary Defects during Grain

Coarsening of Lamellar Block Copolymers. *Macromolecules* **2013**, *46*, 204–215. https://doi.org/10.1021/ma3015382.

(15) Patel, A. J.; Narayanan, S.; Sandy, A.; Mochrie, S. G. J.; Garetz, B. A.; Watanabe, H.; Balsara, N. P. Relationship between Structural and Stress Relaxation in a Block-Copolymer Melt. *Phys. Rev. Lett.* **2006**, *96*, 1–4. https://doi.org/10.1103/PhysRevLett.96.257801.

(16) Oparaji, O.; Narayanan, S.; Sandy, A.; Ramakrishnan, S.; Hallinan, D. Structural Dynamics of Strongly Segregated Block Copolymer Electrolytes. *Macromolecules* **2018**, *51*, 2591–2603. https://doi.org/10.1021/acs.macromol.7b01803.

(17) Nogales, A.; Fluerasu, A. X Ray Photon Correlation Spectroscopy for the Study of Polymer Dynamics. *Eur. Polym. J.* **2016**, *81*, 494–504. https://doi.org/10.1016/j.eurpolymj.2016.03.032.

(18) Lewis, III, R. M.; Beech, H. K.; Jackson, G. L.; Maher, M. J.; Kim, K.; Narayanan, S.; Lodge, T. P.; Mahanthappa, M. K.; Bates, F. S. Dynamics of a Supercooled Disordered Sphere-Forming Diblock Copolymer as Determined by X-Ray Photon Correlation and Dynamic Mechanical Spectroscopies. *ACS Macro Lett.* **2018**, *7*, 1486–1491. https://doi.org/10.1021/acsmacrolett.8b00740.

(19) Jang, W.-S.; Koo, P.; Sykorsky, M.; Narayanan, S.; Sandy, A.; Mochrie, S. G. J. The Static and Dynamic Structure Factor of a Diblock Copolymer Melt via Small-Angle X-Ray Scattering and X-Ray Photon Correlation Spectroscopy. *Macromolecules* **2013**, *46*, 8628–8637. https://doi.org/10.1021/ma4014548.

(20) Patel, A. J.; Mochrie, S. G. J.; Narayanan, S.; Sandy, A.; Watanabe, H.; Balsara, N. P. Dynamic Signatures of Microphase Separation in a Block Copolymer Melt Determined by X-Ray Photon Correlation Spectroscopy and Rheology. *Macromolecules* **2010**, *43*, 1515–1523. https://doi.org/10.1021/ma902343m.

(21) Sanz, A.; Ezquerra, T. A.; Hernández, R.; Sprung, M.; Nogales, A. Relaxation Processes in a Lower Disorder Order Transition Diblock Copolymer. *J. Chem. Phys.* **2015**, *142*, 064904. https://doi.org/10.1063/1.4907722.

(22) Lewis, III, R. M.; Jackson, G. L.; Maher, M. J.; Kim, K.; Lodge, T. P.; Mahanthappa, M. K.; Narayanan, S.; Bates, F. S. A New Framework for X-Ray Photon Correlation Spectroscopy Analysis from Polycrystalline Materials. *Rev. Sci. Instrum.* **2018**, *89*. https://doi.org/10.1063/1.5051451.

(23) Lewis, III, R. M.; Arora, A.; Beech, H. K.; Lee, B.; Lindsay, A. P.; Lodge, T. P.; Dorfman, K. D.; Bates, F. S. Role of Chain Length in the Formation of Frank-Kasper Phases in Diblock Copolymers. *Phys. Rev. Lett.* **2018**, *121*, 208002. https://doi.org/10.1103/PhysRevLett.121.208002.

(24) Wang, X.; Dormidontova, E. E.; Lodge, T. P. The Order-Disorder Transition and the Disordered Micelle Regime for Poly(Ethylenepropylene-b-Dimethylsiloxane) Spheres. *Macromolecules* **2002**, *35*, 9687–9697. https://doi.org/10.1021/ma021009j.

(25) Srivastava, S.; Agarwal, P.; Mangal, R.; Koch, D. L.; Narayanan, S.; Archer, L. A. Hyperdiffusive Dynamics in Newtonian Nanoparticle Fluids. *ACS Macro Lett.* **2015**, *4*, 1149–1153. https://doi.org/10.1021/acsmacrolett.5b00319.

(26) Caronna, C.; Chushkin, Y.; Madsen, A.; Cupane, A. Dynamics of Nanoparticles in a Supercooled Liquid. *Phys. Rev. Lett.* **2008**, *100*, 8–11. https://doi.org/10.1103/PhysRevLett.100.055702.

(27) Berne, B. J.; Pecora, R. *Dynamic Light Scattering with Applications to Chemistry, Biology, and Physics*; John Wiley & Sons, Inc.: New York, 1976.

(28) Gutt, C.; Ghaderi, T.; Chamard, V.; Madsen, A.; Seydel, T.; Tolan, M.; Sprung, M.; Grübel, G.; Sinha, S. K. Observation of Heterodyne Mixing in Surface X-Ray Photon Correlation Spectroscopy Experiments. *Phys. Rev. Lett.* **2003**, *91*, 076104. https://doi.org/10.1103/PhysRevLett.91.076104.

(29) Lhermitte, J. R. M.; Rogers, M. C.; Manet, S.; Sutton, M. Velocity Measurement by Coherent X-Ray Heterodyning. *Rev. Sci. Instrum.* **2017**, *88*. https://doi.org/10.1063/1.4974099.

(30) Ulbrandt, J. G.; Rainville, M. G.; Wagenbach, C.; Narayanan, S.; Sandy, A. R.; Zhou, H.; Ludwig, K. F.; Headrick, R. L. Direct Measurement of the Propagation Velocity of Defects Using Coherent X-Rays. *Nat. Phys.* **2016**, *12*, 794–799. https://doi.org/10.1038/nphys3708.

(31) Choi, S.-H.; Bates, F. S.; Lodge, T. P. Molecular Exchange in Ordered Diblock Copolymer Micelles. *Macromolecules* **2011**, *44*, 3594–3604. https://doi.org/10.1021/ma102788v.

(32) Kremer, K.; Robbins, M. O.; Grest, G. S. Phase Diagram of Yukawa Systems: Model for Charge-Stabilized Colloids. *Phys. Rev. Lett.* **1986**, *57*, 2694–2697.

https://doi.org/10.1103/PhysRevLett.57.2694.

(33) Hartschuh, R. D.; Kisliuk, A.; Novikov, V.; Sokolov, A. P.; Heyliger, P. R.; Flannery, C. M.; Johnson, W. L.; Soles, C. L.; Wu, W. L. Acoustic Modes and Elastic Properties of Polymeric Nanostructures. *Appl. Phys. Lett.* **2005**, *87*, 1–3. https://doi.org/10.1063/1.2119414.

(34) Urbas, A. M.; Thomas, E. L.; Kriegs, H.; Fytas, G.; Penciu, R. S.; Economou, L. N. Acoustic Excitations in a Self-Assembled Block Copolymer Photonic Crystal. *Phys. Rev. Lett.* **2003**, *90*, 108302-1–4. https://doi.org/10.1103/PhysRevLett.90.108302.

(35) Cheng, W.; Gomopoulos, N.; Fytas, G.; Gorishnyy, T.; Walish, J.; Thomas, E. L.; Hiltner, A.; Baer, E. Phonon Dispersion and Nanomechanical Properties of Periodic 1D Multilayer Polymer Films. *Nano Lett.* **2008**, *8*, 1423–1428. https://doi.org/10.1021/nl080310w.

(36) Lee, J. H.; Koh, C. Y.; Singer, J. P.; Jeon, S. J.; Maldovan, M.; Stein, O.; Thomas, E. L. 25th Anniversary Article: Ordered Polymer Structures for the Engineering of Photons and Phonons. *Adv. Mater.* **2014**, *26*, 532–569. https://doi.org/10.1002/adma.201303456.

(37) Lu, J.; Aabdin, Z.; Loh, N. D.; Bhattacharya, D.; Mirsaidov, U. Nanoparticle Dynamics in a Nanodroplet. *Nano Lett.* **2014**, *14*, 2111–2115. https://doi.org/10.1021/nl500766j.

(38) Dake, J. M.; Oddershede, J.; Sørensen, H. O.; Werz, T.; Shatto, J. C.; Uesugi, K.; Schmidt, S.; Krill, C. E. Direct Observation of Grain Rotations during Coarsening of a Semisolid Al-Cu Alloy. *Proc. Natl. Acad. Sci. U. S. A.* **2016**, *113*, E5998–E6006. https://doi.org/10.1073/pnas.1602293113.

(39) Harris, K. E.; Singh, V. V.; King, A. H. Grain Rotation in Thin Films of Gold. *Acta*

Mater. **1998**, *46*, 2623–2633.

(40) Moldovan, D.; Wolf, D.; Phillpot, S. R. Theory of Diffusion-Accommodated Grain Rotation in Columnar Polycrystalline Microstructures. *Acta Mater.* **2001**, *49*, 3521–3532. https://doi.org/10.1016/S1359-6454(01)00240-3.

(41) Gabriel, J.; Blochowicz, T.; Stühn, B. Compressed Exponential Decays in Correlation Experiments: The Influence of Temperature Gradients and Convection. *J. Chem. Phys.* **2015**, *142*. https://doi.org/10.1063/1.4914092.

(42) Balsara, N. P.; Garetz, B. A.; Chang, M. Y.; Dai, H. J.; Newstein, M. C.; Goveas, J. L.; Krishnamoorti, R.; Rai, S. Identification of the Molecular Parameters That Govern Ordering Kinetics in a Block Copolymer Melt. *Macromolecules* **1998**, *31*, 5309–5315. https://doi.org/10.1021/ma980457h.

(43) Chastek, T. Q.; Lodge, T. P. Grain Shapes and Growth Kinetics during Self-Assembly of Block Copolymers. *J. Polym. Sci. Part B Polym. Phys.* **2006**, *44*, 481–491. https://doi.org/10.1002/polb.20718.

(44) Spencer, R. K. W.; Curry, P. F.; Wickham, R. A. Nucleation of the BCC Phase from Disorder in a Diblock Copolymer Melt: Testing Approximate Theories through Simulation. *J. Chem. Phys.* **2016**, *145*, 144902. https://doi.org/10.1063/1.4964631.

(45) Leibig, C. M.; Fredrickson, G. H. Tracer Diffusion in Fluctuating Block Copolymer Melts. *J. Polym. Sci. Part B Polym. Phys.* **1996**, *34*, 163–171. https://doi.org/10.1002/(SICI)1099-0488(19960115)34:1<163::AID-POLB14>3.0.CO;2-C.

(46) Goveas, J. L.; Milner, S. T. Dynamics of the Lamellar-Cylindrical Transition in Weakly Segregated Diblock Copolymer Melts. *Macromolecules* **1997**, *30*, 2605–2612. https://doi.org/10.1021/ma9611811.

(47) Headrick, R. L.; Ulbrandt, J. G.; Myint, P.; Wan, J.; Li, Y.; Fluerasu, A.; Zhang, Y.; Wiegart, L.; Ludwig, K. F. Coherent X-Ray Measurement of Step-Flow Propagation during Growth on Polycrystalline Thin Film Surfaces. *Nat. Commun.* **2019**, *10*, 1–9. https://doi.org/10.1038/s41467-019-10629-8.

(48) Liu, Y.; Nie, H.; Bansil, R.; Steinhart, M.; Bang, J.; Lodge, T. P. Kinetics of Disorder-to-Fcc Phase Transition via an Intermediate Bcc State. *Phys. Rev. E - Stat. Nonlinear, Soft Matter Phys.* **2006**, *73*, 1–6. https://doi.org/10.1103/PhysRevE.73.061803.

(49) Gottstein, G.; Molodov, M. A.; Shvindlerman, L. S.; Srolovitz, D. J.; Winning, M. Grain Boundary Migration: Misorientation Dependence. *Curr. Opin. Solid State Mater. Sci.* **2001**, *5*, 9–14. https://doi.org/10.1016/S1359-0286(00)00030-9.

(50) Upmanyu, M.; Srolovitz, D. J.; Shvindlerman, L. S.; Gottstein, G. Misorientation Dependence of Intrinsic Grain Boundary Mobility: Simulation and Experiment. *Acta Mater.* **1999**, *47*, 3901–3914. https://doi.org/10.1016/S1359-6454(99)00240-2.

(51) Lavergne, F. A.; Aarts, D. G. A. L.; Dullens, R. P. A. Anomalous Grain Growth in a Polycrystalline Monolayer of Colloidal Hard Spheres. *Phys. Rev. X* **2017**, *7*, 1–13. https://doi.org/10.1103/PhysRevX.7.041064.

(52) Hutchinson, W. B.; Ryde, L.; Bate, P. S.; Bacroix, B. On the Description of Misorientations and Interpretation of Recrystallisation Textures. *Scr. Mater.* **1996**, *35*,

579–582. https://doi.org/10.1016/1359-6462(96)00194-7.

(53) Gillard, T. M.; Lee, S.; Bates, F. S. Dodecagonal Quasicrystalline Order in a Diblock Copolymer Melt. *Proc. Natl. Acad. Sci.* **2016**, *113*, 5167–5172. https://doi.org/10.1073/pnas.1601692113.

(54) Berardi, C. R.; Barros, K.; Douglas, J. F.; Losert, W. Direct Observation of Stringlike Collective Motion in a Two-Dimensional Driven Granular Fluid. *Phys. Rev. E - Stat. Nonlinear, Soft Matter Phys.* **2010**, *81*, 041301. https://doi.org/10.1103/PhysRevE.81.041301.

(55) Zhang, H.; Srolovitz, D. J.; Douglas, J. F.; Warren, J. A. Grain Boundaries Exhibit the Dynamics of Glass-Forming Liquids. *Proc. Natl. Acad. Sci. U. S. A.* **2009**, *106*, 7735–7740. https://doi.org/10.1073/pnas.0900227106.

(56) Niu, L. L.; Zhang, Y.; Shu, X.; Jin, S.; Zhou, H. B.; Gao, F.; Lu, G. H. Interplay between Intrinsic Point Defects and Low-Angle Grain Boundary in Bcc Tungsten: Effects of Local Stress Field. *J. Phys. Condens. Matter* **2015**, *27*. https://doi.org/10.1088/0953-8984/27/25/255007.

(57) Arakawa, K.; Ono, K.; Isshiki, M.; Mimura, K.; Uchikoshi, M.; Mori, H. Observation of the One-Dimensional Diffusion of Nanometer-Sized Dislocation Loops. *Science.* **2007**, *318*, 956–959. https://doi.org/10.1126/science.1145386.

(58) Sanborn, C.; Ludwig, K. F.; Rogers, M. C.; Sutton, M. Direct Measurement of Microstructural Avalanches during the Martensitic Transition of Cobalt Using Coherent X-Ray Scattering. *Phys. Rev. Lett.* **2011**, *107*, 1–4.

https://doi.org/10.1103/PhysRevLett.107.015702.